Ultrasonics Sonochemistry 76 (2021) 105664

Contents lists available at ScienceDirect

Ultrasonics Sonochemistry

journal homepage: www.elsevier.com/locate/ultson

The impact of ultrasonic parameters on the exfoliation of NiFe LDH nanosheets as electrocatalysts for the oxygen evolution reaction in alkaline media

Tshimangadzo S. Munonde [a,b], Haitao Zheng [a,*]

[a] Energy Centre, Council for Scientific and Industrial Research (CSIR), P.O Box 395, Pretoria 0001, South Africa
[b] Department of Chemical Sciences, University of Johannesburg, Doornfontein Campus, P.O Box 17011, Johannesburg 2028, South Africa

ARTICLE INFO

Keywords:
NiFe LDH
Nanosheets
Exfoliation
OER
Ultrasonication
Water

ABSTRACT

The ultrasonic process has been examined to exfoliate layered materials and upgrade their properties for a variety of applications in different media. Our previous studies have shown that the ultra-sonication treatment in water without chemicals has a positive influence on the physical and electrochemical performance of layered materials and nanoparticles. In this work, we have probed the impact of ultrasonication on the physical properties and the oxygen evolution reaction (OER) of the NiFe LDH materials under various conditions, including suspension concentration (2.5–12.5 mg mL^{-1}), sonication times (3–20 min) and amplitudes (50–90%) in water, in particular, sonication times and amplitudes. We found that the concentration, amplitude and time play significant roles on the exfoliation of the NiFe LDH material. Firstly, the NiFe LDH nanosheets displayed the best OER performance under ultrasonic conditions with the concentration of 10 mg mL^{-1} (50% amplitude and 15 min). Secondly, it was revealed that the exfoliation of the NiFe LDH nanosheets in a short time (<10 min) or a higher amplitudes (≥80%) has left a cutdown on the OER activity. Comprehensively, the optimum OER activity was displayed on the exfoliated NiFe LDH materials under ultrasonic condition of 60% (amplitude), 10 mg mL^{-1} and 15 min. It demanded only 250 mV overpotentials to reach 10 mA cm^{-2} in 1 M KOH, which was 100 mV less than the starting NiFe LDH material. It was revealed from the mechanism of sonochemistry and the OER reaction that, after exfoliation, the promoted OER performance is ascribed to the enriched Fe^{3+} at the active sites, easier oxidation of Ni^{2+} to Ni^{3+}, and the strong electrical coupling of the Ni^{2+} and Fe^{3+} during the OER process. This work provides a green strategy to improve the intrinsic activity of layered materials.

1. Introduction

Electrochemical water splitting remains an efficient and promising approach to generate clean energy in the form of oxygen and hydrogen fuels [1–3]. Nonetheless, the oxygen evolution reaction (OER) involving a four electron transfer process is kinetically slow, which consequently requires extra potential to drive the reaction [4,5]. Subsequently, a highly effective electrocatalyst is required to advance the reaction kinetics and therefore decrease the overpotential [6,7]. Although the precious metal oxides such as IrO_2 and RuO_2 electrocatalyst have shown substantial electrocatalytic properties, their high cost limit their large scale applications [8–10]. Alternatively, the fabrication of highly efficient, low cost and prosperous transition metal based OER electrocatalysts have been investigated [11–17]. Amongst the identified alternatives, Layered double hydroxides (LDHs) have shown greater potential owing to their unique tunable metal species, exchangeable interlayer spacing and excellent catalytic performances [18,19], especially in the oxygen evolution reaction (OER) in alkaline media [2,20–22]. The intensive researches were found on NiFe LDH as electrocatalysts for water electrolysis [5,10,21,23–25]. The initial synthesized NiFe LDH materials possess stacked nanosheets that limited exposure of catalytically active sites. However, the most researches are focused on incorporating carbon materials with NiFe LDH to elevate charge transfer kinetics and further improve the catalytic activity [26–28]. Obviously, the lack of attention is paid to the expansion of active sites or intrinsic activity of the NiFe LDH electrocatlyst. Accordingly, it is critical to initialize the packed basal planes for escalating the catalytic activity of the NiFe LDH. Eventually, some interesting findings

* Corresponding author.
E-mail address: hzheng@csir.co.za (H. Zheng).

https://doi.org/10.1016/j.ultsonch.2021.105664
Received 25 January 2021; Received in revised form 4 June 2021; Accepted 4 July 2021
Available online 7 July 2021

show that the electrochemical performance of the LDH material was enhanced after being exfoliated into single or thinner nanosheets. It is believed that exfoliation exposes more active sites, which leading to increased mass transfer, accelerating electron transfer, and stronger structural stability [29–31]. In general, the most exfoliation processes for layered materials mainly involved chemical methods (liquid-phase with various organic or inorganic solvents) and mechanical methods (sonication, ball milling and fluid dynamics) [32]. Recently, the use of sonochemistry for the synthesis of catalysts, especially as energy materials has offered many merits in the light of rapidity, simplicity, efficiency, and environmentally friendliness. [33–35]. In the other hand, the morphology of nanomaterials can be affected greatly by ultrasonication time, power, frequency and as well as the solution volume [36–38]. Furthermore, regarding the effect of ultrasonic condition, Yadav et al. [39] indicated that during the $MnFe_2O_4$ synthesis, the sonication time and percentage of amplitude have significantly affected the structural, cationic distribution and physical property of the $MnFe_2O_4$. In addition, Cai et al. [40] have investigated the effects of sonication power and time on generating graphene nanoplatelets from graphite using liquid-phase exfoliation. A remarkable finding was that the bulk graphene, h-BN, MoS_2, WS_2 and $MoSe_2$ layered materials can be ultrasonic exfoliated into atomically thin platelets in pure water[41]. The authors observed that apart from low cost, the method not only favor exfoliation, but also leads to high dispersion stability. However, the method involves a very long sonication period of 60 h in a bath ultrasound. Our recent work show that ultrasonic treatment on nanomaterials in water in a short time (10 min) have a great impact on the properties and the electrochemical performance of $NiFe_2O_4$/C and $CoFe_2O_4$/C nanoparticles [42,43]. However, to the best of our knowledge, there are no detailed reports on the roles of the ultrasonic parameters play in the exfoliation of layer materials using water as media.

From our previous study, we have observed that carbon has a negative influence on the exfoliation of the NiFe LDH/C layer materials [44]. To limit the carbon interference, in this work, we explore the effect of ultrasonic condition on the properties of the NiFe LDH materials without carbon additives as well as electrocatalyst for OER. The NiFe LDH concentration in water, percentage of amplitude and sonication time were investigated in detail.

2. Experimental section

2.1. Synthesis of NiFe LDH materials and the procedures of the ultrasonic exfoliation

The preparation of NiFe LDH followed the same method as our previous study without carbon additives [44] (seen details in Supplementary). The Ni:Fe molar ratio was ~ 2.6:1.

The ultrasonic exfoliation was conducted using tip sonication (UIP500hd-230, Hielscher). The synthesized materials were exfoliated in deionised water under various conditions. After exfoliation, the 0.5 mL NiFe LDH suspension was dispensed into 1.5 mL of the prepared Nafion aqueous solution to make the ink which was then deposited onto the GC electrode.

The ultrasonic exfoliation was performed in various concentrations of NiFe LDH suspension with the value of 2.5, 5.0, 7.5, 10 and 12.5 mg mL^{-1} at 50% amplitude (named as 50A) for 15 min.

To optimize the sonication time, five aqueous NiFe LDH suspensions with concentration of 10 mg mL^{-1} were sonicated for 3, 5, 10, 15 and 20 min, respectively, under 50% amplitude.

Following the optimizations of concentration and sonication time, five suspensions with each concentration of 10 mg mL^{-1} were sonicated under the different ultrasound amplitude (50–90%) for 15 min.

2.2. Characterization

The physical properties of the synthesized materials were characterised using the following instruments: the transmission electron microscopy (TEM, JEM-2100, JEOL, Tokyo, Japan). Scanning electron microscopy (SEM-EDX, Auriga Cobra FIB FE-SEM, Germany). Fourier transform infrared spectrometer (Waltham, MA, USA), The X-ray diffractometer (XRD, λ = 0.15406 nm, Rigaku). X-ray photoelectron spectroscopy (XPS) and Thermogravimetric analysis (TGA,NETZSCH, STA 429CD analyser, Germany. 20–900 °C in a nitrogen atmosphere.

2.3. Electrochemical measurements

The electrochemical performances were conducted on an AUTOLAB (PGSTAT 302) with a three-electrode system, the counter and reference electrode used were platinum rod and Ag/AgCl, respectively. The glassy carbon (GC) electrode (3 mm in diameter) was used as the working electrode. The loadings of the catalyst were ca. 0.16 mg cm^{-2}. The linear sweep voltammetric (LSV) data were measured after activation of the catalyst with cyclic voltammetric (CV) experiments. Electrochemical impedance spectroscopy (EIS) was tested between 0.1 to10^5 Hz at 1.5 V vs RHE. Cyclic voltammetry was conducted at scan rates of 5 to 50 mV s^{-1} for the estimation of the electrochemical surface area (ECSA) through the double layer capacitance (C_{dl}). The chronopotentiometric measurements were conducted on Ni foam (working electrode) with electrocatalysts loaded at the current of 10 mA cm^{-2}. The iR corrected potentials were converted to RHE (reversible hydrogen electrode) by the equation: $E_{RHE} = E_{Ag/AgCl} + 0.059\ pH + E^{\circ}_{Ag/AgCl}$, where: $E^{\circ}_{Ag/AgCl} = 0.1976$ V (1).

3. Results and discussion

This work mainly focuses on the effects of ultrasonic amplitude and sonication time (due to space limitations) on the OER activity of the NiFe LDH electrocatalysts in 1 M KOH. Previously, the concentration of the NiFe LDH was optimised in water at 50% amplitude for 15 min, as presented in **Fig.S1**(Supplementary) and the OER activities were summarized in **Table S1**(Supplementary). The sample with concentration of 10 mg mL^{-1} demonstrates the best OER performance. Therefore, the concentration of 10 mg mL^{-1} was used as a constant while investigating effect of the amplitude and exfoliation time.

The SEM images, and XRD patterns of the original NiFe LDH and the Exf NiFe LDH materials at different conditions were shown in Fig. 1. From Fig. 1**a**, the pristine NiFe LDH show stacked nanosheets with larger sizes with the range of ~ 70–800 nm and a thickness ranging from ~ 25 to ~ 40 nm. After exfoliation, the sizes and thickness of the Exf NiFe LDH materials were significantly decreased, in particular, under low power input (50A-60A) and short time (10–15 min), with narrowed sizes ranging from ~ 30–300 nm and a thickness of ~ 12–20 nm (Fig. 1 **(1b, 1c)),** indicating that the stacked NiFe LDHs had been successfully exfoliated by ultrasonication in water. However, the stacked nanosheets resurfaced after a long sonication time (20 min) (Fig. 1**c**) or high power input (80A) (Fig. 1**d**), because high sonication amplitude and longer sonication times promote aggregation that leading to the inconsistent exfoliation [40,41].

The XRD patterns in Fig. 1**f** indicate the typical characteristic peaks of the NiFe LDH on all the samples at 11.3°, 22.6°, 33.1°, 34.2°, 35.2°, 38.3°, 46.3°, 60.1° and 61.1°, indexed as (003), (006), (101), (012), (009), (015), (018), (110) and (113), respectively, that were matched to the NiFe LDH material (JCPDS card No. 40–0215)[46,47]. The peaks at 39.2°, 52.2° and 62.8° correspond to the (101), (012) and (111) planes of β-$Ni(OH)_2$ (JCPDS card no. 14–0117) [4]. Additionally, the diffraction peaks at 16.4°, 26.7°, 43.1°, 55.9° and 67.9° indexed as (200), (310), (321), (521) and (312) can be attributed to β-FeOOH (JCPDS 75–1549), resulting from the possible hydrolysis of Fe(III) in solution [48]. After exfoliation, the (003), (310), (321) and (018) diffraction peaks became sharper with increased intensities in all exfoliated materials, which indicates increased periodicity in these crystallographic directions, which is the typical character of LDHs [3].

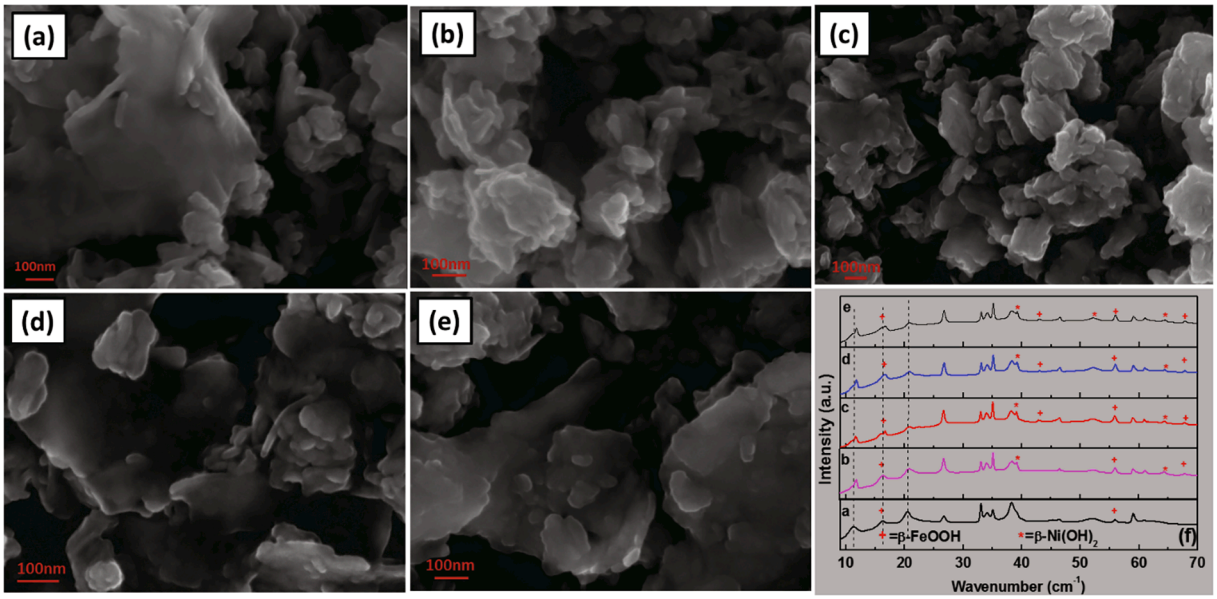

Fig. 1. SEM images (a-e) and XRD patterns (f) of NiFe LDH and Exf- NiFe LDH under different sonication conditions; (The pristine NiFe LDH (a); Exf- NiFe LDH (b, 10mins, 50A; c, 15mins, 60A; d, 20 min, 60A; e, 15mins, 80A).

Meanwhile, the basal peaks are shifted. This indicates the increase in the intercalation anions (CO_3^{2-}) that were detached from the surface into the interlayer space leading to an extension on the interlayer distance, which signifies a successful exfoliation process [49–51]. Additionally, the interlayer spacing was calculated by the Bragg's law based on the (003) planes, the value of interlayer spacing is 0.747 for the pristine NiFe LDH, and 0.751, 0.781, 0.751, 0.753 nm for Exf- NiFe LDH under different conditions (10mins, 50A), (15mins, 60A), (20 min, 60A), (15mins, 80A), respectively. It can be seen that interlayer spacing is increased after exfoliation, the largest interlayer spacing is display in the Exf- NiFe LDH under the mild condition (15mins, 60A). **Fig.S3g** show the elements mappings of Ni, Fe and O as the main components in all the samples. All the three elements have shown similar patterns with a homogeneous distribution on each sample. Table 1 in Fig. 1 shows the EDX analysis extracted from **Fig.S3**. It is worth noting that the atomic ratio of Ni/Fe is 3.2 on the pristine NiFe LDH that is higher than the original experimental ratio of 2.6, which implies the possible loss of Fe ions during the synthesis. After exfoliation, the ratio of Ni/Fe dramatically decreased to 1.1–1.4, which was probably due to the ultrasound power that detached Ni^{2+} from the surface and varied according to the ultrasonic condition and the compounds stabilities [52,53]. As an evidence from the water changed to greenish solution after the ultrasonication. However, specific effect of the ultrasonic condition on the ratio of Ni/Fe still need to be further investigated.

Further insights on the morphology of the NiFe LDH and the Exf NiFe LDH were explored using TEM /SAED as shown in Fig. 2. The Exf NiFe LDH (15 min, 60%) as an example to compare with the pristine NiFe LDH as the SEM images have shown a negligible difference among the exfoliated samples. The comparison from Fig. 2 clearly shows that the stacked nanosheets of the pristine NiFe LDH were successfully exfoliated into mono- and thinner layered sheets. Fig. 2**b** displays the multilayer nanosheets of the pristine NiFe LDH (≥23layers) in the measurement range, with a thickness of ~ 5 nm in a thinnest nanosheets. Successively, Fig. 2**c** shows the mono/few layer nanosheets of the Exf NiFe LDH, with a thickness of ~ 0.227 nm in a monolayer.

The SAED pattern of the Exf NiFe LDH (Fig. 2**f**) shows more prominent diffraction rings with brighter spots than those of the NiFe LDH (Fig. 2**c**), indicating an increased orientation degree leading to an increased conductivity after the ultrasonic exfoliation into mono/few layer nanosheets [54,55], which is related to increased intensities of some peaks in XRD [56,57]. This is reflected by the first four diffraction rings that were found to correspond to the (009), (012), (113) and (118) facets observed on the XRD, indicating the retention of the crystalline structure after exfoliation.

To further elucidate the chemical structures of the NiFe LDH and the Exf NiFe LDH materials, FTIR spectra was illustrated in Fig. 3. In Fig. 3**A**, the broad bands observed around 3300–3500 cm^{-1} can be allocated to the O–H stretching vibrations in the brucite-like layers [27]. The 2185 cm^{-1} band can be assigned to the C-O vibrations emanating from the CO_3^{2-} anions [28]. The 1621 cm^{-1} band can be attributed to vibrations of the cohering H_2O molecules [58]. The 1345 cm^{-1} band belong to the intercalated CO_3^{2-} anions vibrations [28,58]. The presence of the intrinsic stretching vibrations of Fe-O, Ni-O and Ni-O-Fe bonds in all NiFe LDH materials are confirmed by the characteristic peaks between 400 and 700 cm^{-1} (Fig. 3**B**) [27,58]. The reduced intensity of CO_3^{2-} band observed in all exfoliated materials due to the increased inter-layer spacing as a result of forming mono-/few layer sheets after exfoliation [49,59]. After exfoliation, the metal–oxygen (M−O) bands around 640 cm^{-1} and 450 cm^{-1} became weaker, suggesting a decrease in the metal–oxygen bonding (Fig. 2B). Meanwhile, the band of 450 cm^{-1} shifts to low energy. In addition, the M−O bands around 450 cm^{-1} show the decrease of the intensities with narrower peaks. Comprehensively, the CO_3^{2-} bands and the M−O bands are reduced after ultrasonication, indicating the exfoliation of the NiFe LDH occurred during ultrasonication in water.

The thermal behaviour of the NiFe LDH and the Exf NiFe LDH were evaluated by TGA/DTA in Fig. 4. The TGA (Fig. 4**a**) and DTA (Fig. 4**b**) curves show two-steps weight loss on the pristine and two of the Exf-NiFe LDH with longer time (20 min) and high amplitude (80A). However, the rest of the Exf NiFe LDH materials show two main steps with small multi-steps. On the first main step, the weight loss arose at about

Table 1
Summary of EDX analysis.

Sample	Pristine NiFeLDH	Exf- NiFeLDH Exfoliation condition			
		10mins (50A)	20mins (50A)	60A (15mins)	80A (15mins)
Ratio of Ni:Fe	3.2:1	1.1:1	1.0:1	1.3:1	1.4:1

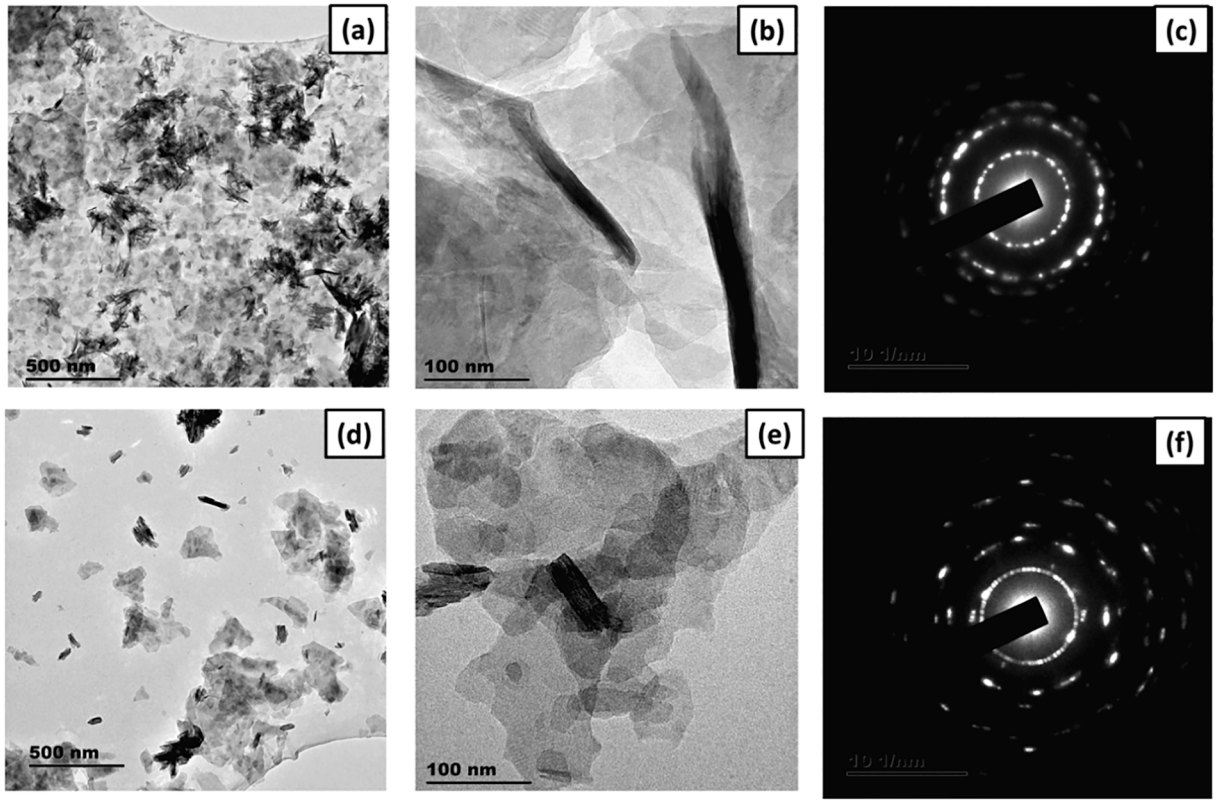

Fig. 2. TEM and SAED patterns of NiFe LDH (a-c) and Exf NiFe LDH (15 min, 60%) (d-f).

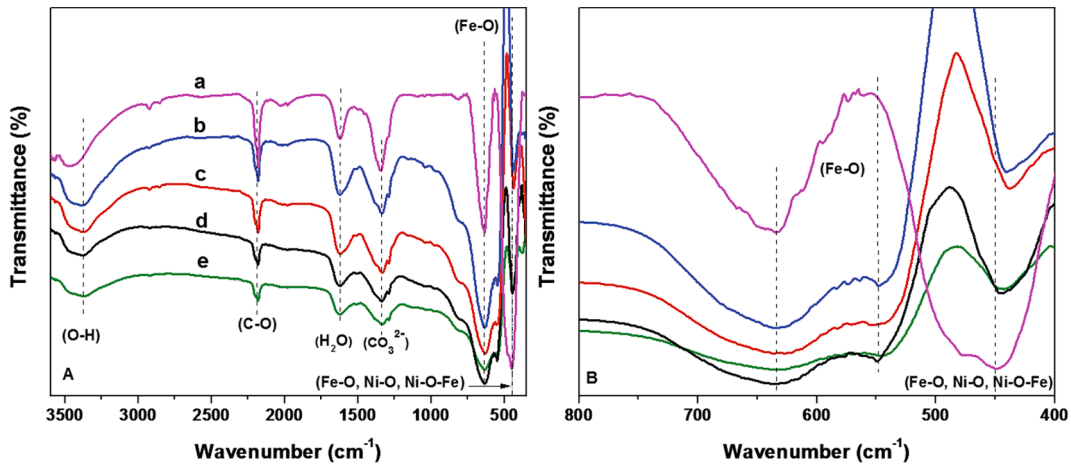

Fig. 3. FTIR spectra of NiFe LDH (a) and Exf NiFe LDH (b-e) with full range wavenumber (A) and low wavenumber (B). Exf NiFe LDH under different conditions (b, 10 min, 50A; c, 10 min, 50A; d, 60A,15 min; e, 80A, 15 min).

220℃, which is ascribed to the removals of the surface and intercalated water molecules. Further weight loss belongs to the decomposition and elimination of interlayer CO_3^{2-} anions, as well as the dehydroxylation of metal hydroxide layers to metal oxides [34,40,44]. Furthermore, the Exf NiFe LDH with a short time (10 min) and low amplitude (60A) has shown extra steps around 240-290℃ and around 400℃ that emancipates from the β-Ni(OH)$_2$ and β-FeOOH indicated in the XRD. The total weight loss of the NiFe LDH is 23.5% at 800℃. However, the weight loss of the Exf NiFe LDH under different conditions with varying degrees of weight loss can be ascribed to the high amount of intercalated water and anions freed from the LDH surface during exfoliation [60,61]. The order of weight loss of all the Exf NiFe LDH at 800℃ is 45.1% (10 min, 50A) > 29.8% (20 min, 50A) > 24.4% (15 min, 80A), which is higher than the initial NiFe LDH with 23.5% loss. The TGA results suggested that the ultrasonic exfoliation had no significant effect on the thermal stability of the NiFe LDH material, and all synthesized materials have shown to be stable below ~ 220℃.

XPS analysis was also evaluated on the NiFe LDH and the Exf NiFe LDH (15 min, 60A), as seen in Fig. 5 and the peaks percentages of the deconvoluted Ni2p, Fe2p, O1s were listed in **Table S2-S4.** The survey spectra in Fig. 5**a** confirm the existence of O, Ni and Fe in all the prepared samples, which is in line with the EDX results. Furthermore, the intensities are reduced after exfoliation in the survey spectra, which is consistent with the weaker energy of the M−O bands after exfoliation from the FTIR results. In Fig. 5**b**, the Ni 2p doublet was deconvoluted into Ni $2p_{3/2}$ and Ni $2p_{1/2}$ located at 853.87 and 871.55 eV, alongside

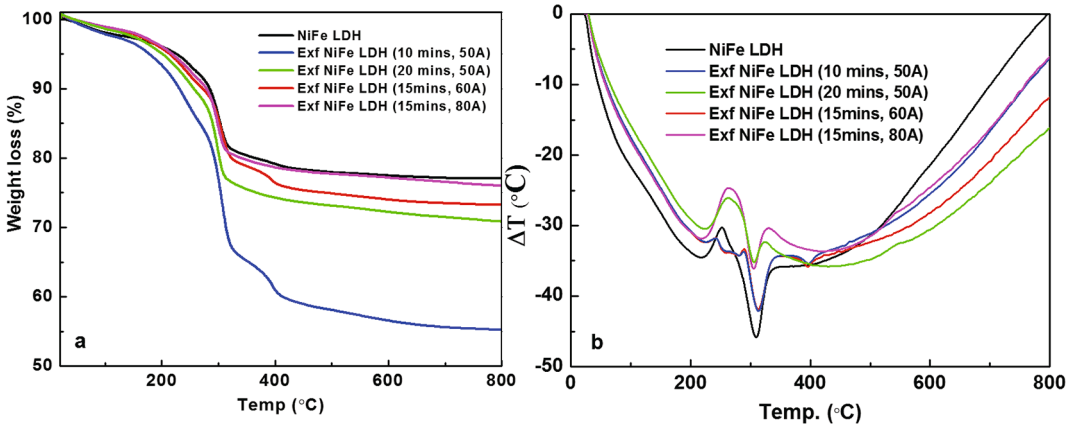

Fig. 4. TGA (a) and DTA (b) curves of NiFe LDH and Exf NiFe LDH.

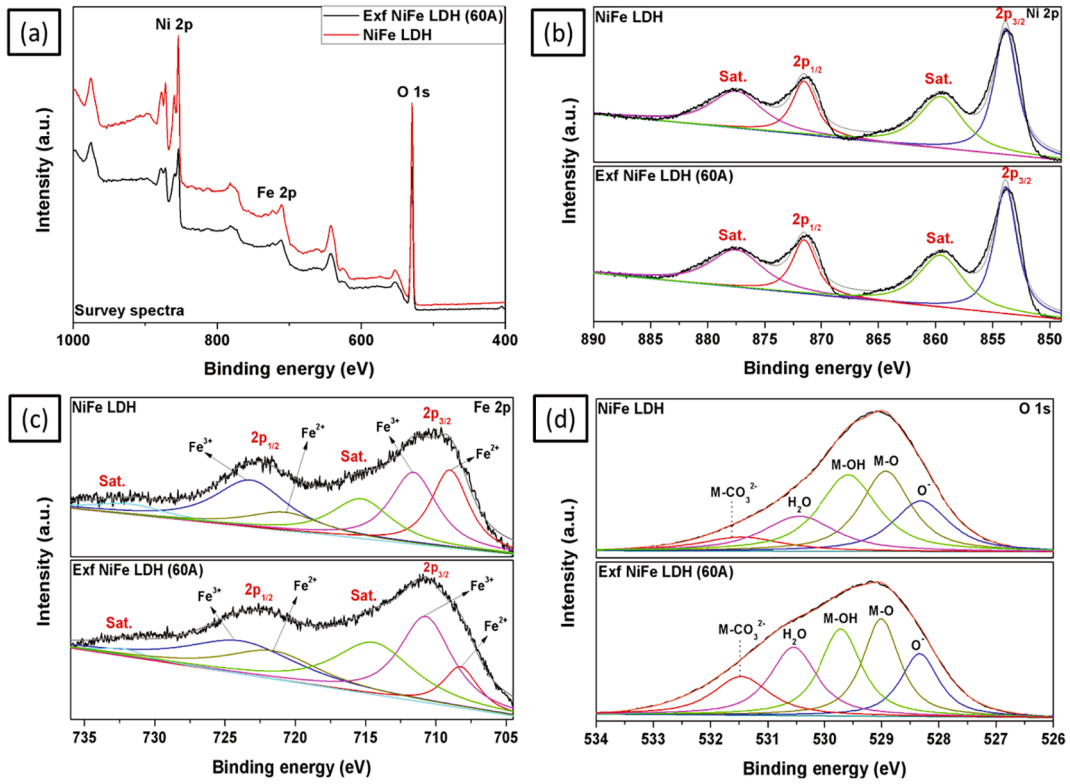

Fig. 5. (a) XPS survey spectra; (b) Ni 2p spectra; (c) Fe 2p spectra; (d) O 1 s spectra of NiFe LDH and Exf NiFe LDH (60A) materials.

two corresponding satellite peaks found at 859.54 and 877.50 eV, highlighting the presence of Ni^{2+} [62]. The Fe 2p deconvoluted doublet (Fig. 5**c**) shows the presence of Fe^{2+} and Fe^{3+} in each of the Fe $2p_{3/2}$ and Fe $2p_{1/2}$ located around 708.99 and 720.70 eV, respectively, alongside two satellite peaks at ~ 715 and ~ 731 eV, indicating the attributes of Fe ions [63]. It is noteworthy that the Fe^{3+} content increased after exfoliation (**Table S3**).During the ultrasonic exfoliation, firstly, water molecules was dissociated by sonolysis to yield hydrogen radicals ($H^{\bullet}$) and hydroxyl radicals ($OH^{\bullet}$) during the bubble collapse triggered by the ultrasonic cavitation in water [36,37,64] (Eq.1). Since the exfoliation was performed under the atmosphere, in the presence of O_2, the $H^{\bullet}$ reacted with O_2 to form $HO^{\bullet}{}_2$ (Eq.2) that suppressed the reaction of the radicals ($H^{\bullet}$ and $OH^{\bullet}$) to recombine to H_2O, remaining with $OH^{\bullet}$ in the solution [65,66]. Furthermore, the $OH^{\bullet}$ radicals combine to form H_2O_2 (Eq.3). Meanwhile, $HO^{\bullet}{}_2$ radicals are re-associated lead to a further increase of H_2O_2 (Eq.4) [67]. Then Fe^{2+} reacted with H_2O_2 to produce Fe^{3+} due to high temperature (ca. 5000 K)/pressure (ca. 2000 atms) generated from the collapsing of cavitation bubbles (Eq.5) [37,68,69].

$$H_2O \rightarrow H^{\bullet}+OH^{\bullet} \quad (1)$$

$$H^{\bullet}+O_2 \rightarrow OH^{\bullet}{}_2 \quad (2)$$

$$OH^{\bullet}+ OH^{\bullet} \rightarrow H_2O_2 \quad (3)$$

$$2HO^{\bullet}{}_2 \rightarrow H_2O_2 + O_2 \quad (4)$$

$$Fe^{2+}+ H_2O_2 \rightarrow Fe^{3+}+OH^{\bullet}+OH^{-} \quad (5)$$

The O 1 s deconvolution (Fig. 5**d**) resulted in five peaks representing the surface labile oxygen (O^{-}, 528.31 eV, metal–oxygen bonds (M−O, 528.93 eV), metal-surface hydroxyl bond (M−OH, 529.58 eV), and surface adsorbed water (H_2O, 530.45 eV) and intercalated anions ($M-CO_3^{2-}$, 531.46 eV). The Exf NiFe LDH showed similar results with

negligible peak position shifts. Interestingly, the intercalated anions ($M-CO_3^{2-}$) doubled after exfoliation (from 7.70 to 14.52%) (**Table S4**), suggesting the exposure of more anions on single/few layer sheets.

3.1. Electrochemical performance

The effects of sonication time and ultrasonic amplitude on the OER performance of the NiFe LDH electrocatalysts were studied in 1 M KOH solution with a constant concentration of 10 mg mL^{-1}. The comparisons were displayed in Figs. 6-8.

3.1.1. Effect of ultrasound-sonication time

The ultrasound-sonication time is one key parameter that plays a very crucial role in the sonication-assisted liquid exfoliation process [39]. We explored the influence of the sonication time (3–20 min) on the OER activity of NiFe LDH nanosheets with the constant amplitude (50%) and concentration (10 mg mL^{-1}). The LSV plot was shown in Fig. 6 and the summary of analysis was listed in **Table S5**. As a reference, the original NiFe LDH was also tested for the OER performance. Noticeably, NiFe LDH catalysts exfoliated for a short period (3–5 min) have shown deterioration on the OER performance when compared with the original NiFe LDH (**Table S5**). It is difficult to explain this phenomenon because its OER activity should be the same as the starting material if exfoliation has not occurred. However, NiFe LDH catalysts exfoliated at prolonged periods (10 min, 15 min and 20 min) have shown improvements on the OER performance when compared to the original NiFe LDH. The prolonged exfoliation period might have increased the inertial cavitation which is responsible for the exfoliation [45]. When the exfoliation time was increased to 15 min, the optimum OER performance was achieved, affording a current density of 10 mA cm^{-2} at the expense of 270 mV overpotential. This result is higher than the Exf NiFe LDH (20 min), Exf NiFe LDH (10 min) and the original NiFe LDH by 20 mV, 40 mV and 80 mV, respectively (see **Table S5**). Additionally, it is obvious that the prolonged exfoliation periods (10–20 min) have caused electron redistribution that made the oxidation of Ni^{2+} to Ni^{3+} easily occur during the OER process as revealed in Fig. 6 [26], which is an active site for OER electrocatalysis [30]. However, over the 15 min exfoliation, the Exf NiFe LDH nanosheets started to agglomerate/fusion occurred as shown in SEM images (Fig. 1), leading to the loss of some exposed active sites [40].

3.1.2. Effect of ultrasound-sonication amplitude

Ultrasound amplitude, as a measure of the acoustic output, is one of the most influential parameters in the ultrasound exfoliation process [70]. The effect of the ultrasonic amplitude (50–90%) was investigated with the concentration of 10 mg mL^{-1} for 15 min, as displayed in Fig. 7 and a summary listed in **Table S6**. Under the 60% exfoliation amplitude, the Exf NiFe LDH shows the lowest overpotential of 250 mV at the current density of 10 mA cm^{-2}, which was 20 mV less than that under the 70% exfoliation amplitude. We can see that the higher ultrasonic amplitudes (80–90%) are not beneficial to the exfoliation of NiFe LDH, requiring 390 and 490 mV overpotentials to drive a current density of 10 mA cm^{-2}, respectively, which was 40 and 149 mV more than the pristine NiFe LDH (**Table S6**). When the high amplitudes were applied on the ultrasonic process that caused the fusion/aggregation of nanosheets instead of exfoliations [45,70,71], as reflected by the SEM images. On the other hand, the Exf NiFe LDH with greater OER performances (50–70% exfoliation amplitude) show a higher Ni^{2+}/Ni^{3+} oxidation peak (inset of Fig. 7), which was believed to influence greatly the OER performance [30].

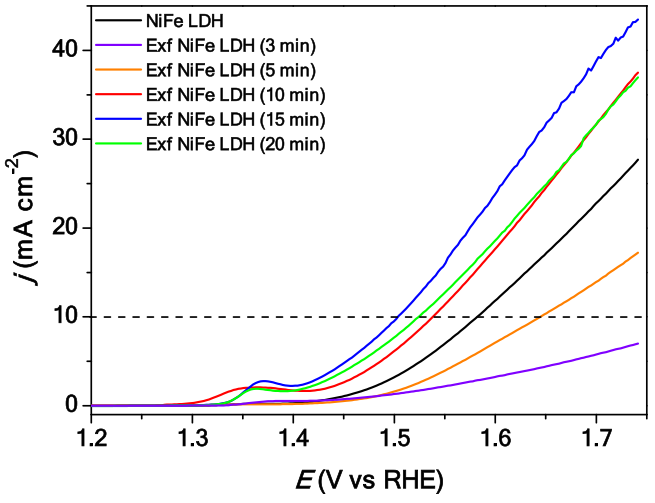

Fig. 6. LSV plots of NiFe LDH and Exf- NiFe LDH with a scan rate of 5 mV s^{-1} at various ultrasound-sonication times (3–20 min) at amplitude of 50% and concentration of 10 mg mL^{-1}.

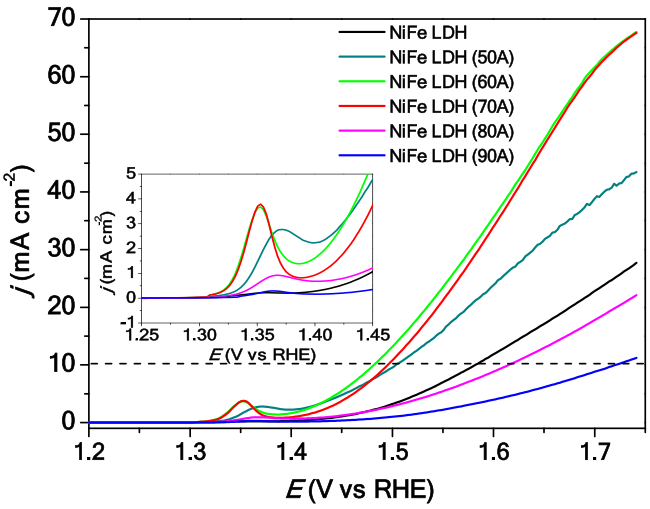

Fig. 7. LSV plots of NiFe LDH with a scan rate of 5 mV s^{-1} exfoliated at a variety of ultrasound-sonication amplitude (50-90A).

Through the optimizations under various conditions, the Exf NiFe LDH (60%, 15 min) was identified as the optimum candidate for the OER performance, which was subjected to further assessment for electrocatalytic performances compared with the pristine NiFe LDH, as exhibited in Fig. 8. From Fig. 8**a**, the Exf NiFe LDH needs 250 mV of overpotential to reach the current density of 10 mA cm^{-2}, which was 100 mV lower than that of the pristine NiFe LDH. This indicates the significant improvement of the OER activity on the NiFe LDH after the exfoliation process. Additionally, the Exf NiFe LDH delivered 3.6 times current density than that of the pristine NiFe LDH at 1.5 V. In addition, this result is superior/comparable to recent studies through alternative approaches to obtain single/thin LDH layers for OER (**Table S7**). The inset graph of Fig. 8**a** depicts the Tafel slopes of the NiFe LDH and the Exf NiFe LDH calculated as 68 and 43 mV dec^{-1}, respectively. The slopes are similar to type A and type B observed in other studies in alkaline solution [72,73], respectively, suggesting the OER kinetic mechanism changed after exfoliation. Obviously, the Exf NiFe LDH with a smaller Tafel slop has a faster electrochemical OER kinetics than that of the original NiFe LDH, which is comparable with the 40 mV dec^{-1} of the benchmark IrO_2 electrocatalyst.

In general, the Tafel slopes of 60 and 40 mV dec^{-1} approximately represent the first and second electron transfer as the rate determining step in the OER with 4 electron transfer process, respectively [74]. Thus, the pristine NiFe LDH (68 mV dec^{-1}) and the Exf NiFe LDH (43 mV dec^{-1}) follow the first and second electron transfer as the rate determining step, respectively. These results strongly suggest the improvement of the charge-transfer process, as indicated by the Nyquist plots in Fig. 8**b**.

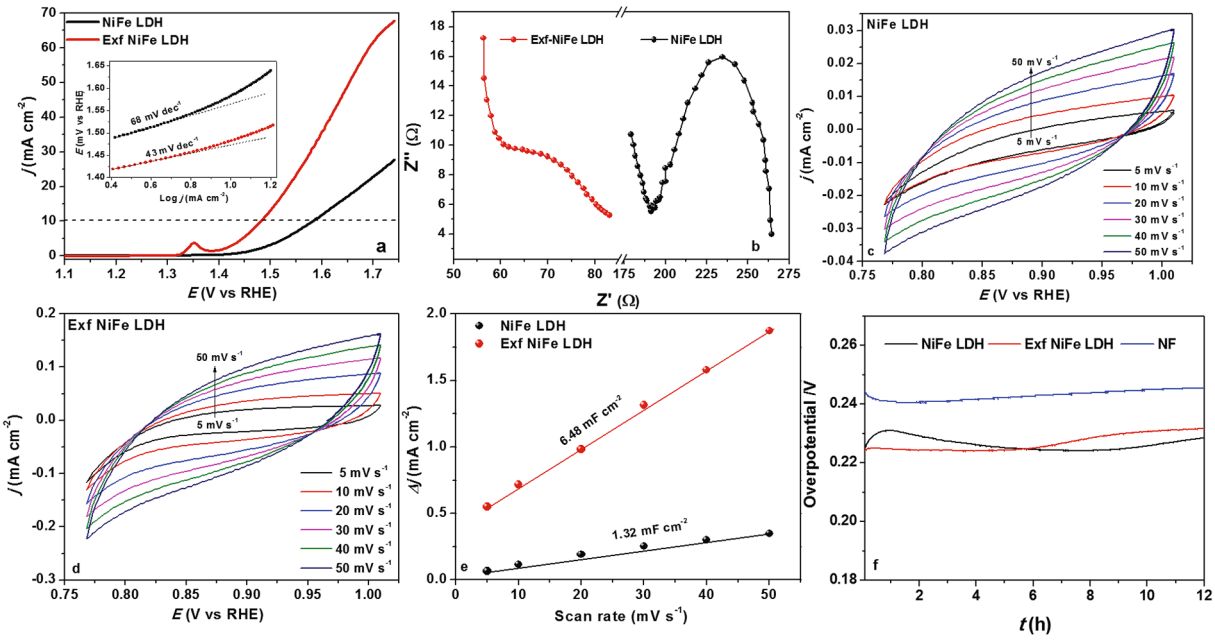

Fig. 8. Electrochemical performance of NiFe LDH and Exf NiFe LDH (60%, 15 min) in 1 M KOH. LSV curves (a) at a scan rate of 5 mV s^{-1} and corresponding Tafel plots (inset of a); Nyquist plots (b); CV curves of NiFe LDH (c), CV curves of Exf NiFe LDH (d), and the capacitive current at potential 0.89 V (vs RHE) as a function of CV scan rate (e); Chronopotentiometric curves at a constant current density of 10 mA cm^{-2} (nickel foam (NF) as a reference)(f).

Fig. 8**b** shows that the Exf NiFe LDH exhibits a much smaller semicircle as opposed to its counterpart of the pristine NiFe LDH. These results indicate the fast electron transfer ability of the Exf NiFe LDH, which is consistent with the Tafel slope analysis. Furthermore, the fast electron transfer ability of the Exf NiFe LDH could be related to the abundantly exposed intrinsic active sites, leading to more adsorption of OH^- on the surface of the Exf NiFe LDH, as there might be virtuous contact between the electrode surface and the electrolyte, benefitting the OER process [1,75,76]. To rationalize this, the electrochemical surface areas (ECSA) were estimated by the CVs at various scan rates (Fig. 8**(d and e)**). The linear slope of the capacitative current against scan rate is illustrated in Fig. 8**e**, which is twice the double-layer capacitance (Cdl), representing the ECSA. [49,75,76]. The Exf NiFe LDH catalyst exhibits the ECSA (6.48 mF cm^{-2}) that was around 5 times larger than that of the pristine NiFe LDH (1.32 mF cm^{-2}), which could have benefitted from the single/thinner nanosheets and was responsible for the higher OER activity [23,49]. This is in concordance with the XRD, FTIR, SEM and TEM results showing the effectiveness of the ultrasonic exfoliation process. Additionally, the unit activity of each site (intrinsic activity) was evaluated by measuring the turnover frequency (TOF) as it influences the OER performance [23]. Assuming that all metal sites are active sites, the TOFs of Exf NiFe LDH (60A) and NiFe LDH were obtained as 0.035 and 0.01 s^{-1}, respectively, indicating better intrinsic activity of the Exf NiFe LDH.

The chronopotentiometry was carried out to evaluate the stability of the OER catalysts for 12 h, as shown in Fig. 8**f**. Nickel form (NF) was used as the working electrode. Thus, a bare NF was tested under the same experimental conditions as a reference. During the first 6 h of the OER process, the Exf NiFe LDH/NF shows a constant overpotential without degradation. However, after 6 h, Exf NiFe LDH/NF shows a slight rise in overpotentials that may be ascribed to a slow release of abundant O_2 gas bubbles from the working electrode [75]. However, the NiFe LDH /NF displays unstable overpotentials with a wave trend during the first 6 h of the OER electrolysis. After 6 h, it kept constant trend for 2 h, then rising slowly again, suggesting the surface passivation of the catalyst under the OER process [77]. Compared to our previous study [44], the exfoliated NiFe LDH/C has shown improved electrochemical stability, although most of the NiFe LDH nanosheets bonding with carbon were not exfoliated. In this work, the exfoliation of the NiFe LDH nanosheets without carbon became easier, however, the exfoliated NiFe LDH without carbon does not benefit the stability.

For the reaction path of the OER in NiFe LDH, it was suggested that OH_{ad} was adsorbed onto the Fe site at a low potential, while at a higher potential, H_{ad} preferred to bind to the Ni site. Hereafter, the reaction intermediates that were generated by adsorbed OH_{ad} reacted with other OH group in alkaline electrolyte, then further oxidized to O_2 and H_2O [78]. Generally, the Fe^{3+} interacted strongly with OH than the Ni^{2+} at a higher potential, as Fe^{3+} is a stronger Lewis acid. Meanwhile, the electronic effect of Fe^{3+} could boost a higher Ni valence, leading to a bond with OH^- that easily promote H_2O dissociation in alkaline solution [26,78]. From the XRD and XPS analysis, the intensity of the (3 1 0) peak of FeOOH (Fe^{3+}) and the percentage of Fe^{3+} after exfoliation was increased, which implies that the water dissociation could be accelerated through the depressing reaction of $Ni(OH)_2$ to NiOOH complex. It was also evident that the OER activity was increased by increasing Fe^{3+} doped in the β-$Ni(OH)_2$ [79]. According to the EDX analysis, the ratio of Ni/Fe was changed remarkably after exfoliation. The changes of Ni^{2+}/Fe^{3+} in the NiFe LDH could be due to the undergoing charge transfer during ultrasonic cavitation. For this reason, the electron density and cationic ions coordination rearranged as the oxidation of Ni^{2+} was boosted consequently and its OER catalytic activity was increased accordingly [80]. In addition, the exfoliation process could be beneficial to the adsorption of the Fe species at the defect or edge sites of the Ni complex, which could effectively improve Ni^{2+} catalytic behaviour [81]. Furthermore, the increased Fe^{3+} could create cation defects in the NiFe LDH after ultrasonication, which can promote the OER performance [82,83]. Most studies show that both Ni and Fe are indispensable in Ni (Co)FeOOH for the OER activity [26,84]. To further understand the Fe role in the OER activity, some advanced characterizations and computational methods were applied on the Ni(Co) Fe (oxy) hydroxides [74,85,86]. The authors claim that Fe^{3+} has a higher intrinsic activity than Ni^{2+} or Co^{2+}, Ni or Co sites in Ni (Co) Fe OOH are the host of Fe rather than active centres for the OER. Additionally, it was suggested that Ni (Co) OOH has a higher electrical conductivity and chemical stability than FeOOH, as strong electrical coupling between Fe and Ni (Co) are essential to the OER activity. In this work, the best OER

performance was obtained on the Exf NiFe LDH with a Ni/Fe ratio of 1.0 that is the lowest ratio From EDX analysis (Table 1 in Fig. 1), which means that the higher Ni/Fe is not beneficial to the OER activity, because Fe occupies the most actives sites.

4. Conclusion

In summary, to explore the impact of the ultrasonic exfoliation, various suspension concentrations, ultrasound amplitudes, and sonication times were conducted for the exfoliation of NiFe LDH, with the OER activity on the respective exfoliated sample tested. It was found that, Firstly, the concentration of 5–10 mg mL^{-1} in water is beneficial to the exfoliation of NiFe LDH nanosheets. Secondly, the short time (<10 min) or high ultrasonic amplitudes (80–90%) show a negative effect on the exfoliation of the NiFe LDH nanosheets, as well as the OER activity. The optimum OER activity was achieved on the sample under exfoliation in a suspension concentration of 10 mg mL^{-1} at an amplitude of 60% for 15 min. The best exfoliated NiFe LDH catalyst shows advanced performance with 250 mV overpotential at a current density of 10 mA cm^{-1}, which is 100 mV less than the initial NiFe LDH catalyst. Furthermore, it was found that Ni^{2+} can be oxidized to Ni^{3+} easily on the exfoliated NiFe LDH, which enhances the OER activity by acting as an active site for OER catalysis. Moreover, the improved OER activity is also as a result of the faster charge transfer on the exfoliated NiFe LDH caused by the Fe and Ni strong electrical coupling. The durability of the exfoliated NiFe LDH nanosheets was maintained similar as the pristine NiFe LDH during the 12 h OER electrolysis. This work provides a green strategy to improve the intrinsic activity of layered materials. To achieve a best catalyst with a balance of activity and stability, we suggest that it is necessary to incorporate suitable amount of carbon or conductive materials into the nanosheets to expand the activity and stability.

CRediT authorship contribution statement

Tshimangadzo S. Munonde: Conceptualization, Methodology, Validation, Formal analysis, Investigation, Writing - original draft, Visualization. **Haitao Zheng:** Conceptualization, Methodology, Investigation, Formal analysis, Writing - review & editing, Visualization, Supervision, Funding acquisition.

Declaration of Competing Interest

The authors declare that they have no known competing financial interests or personal relationships that could have appeared to influence the work reported in this paper.

Acknowledgement

The authors are thankful for the financial support from the CSIR and the National Research Foundation of South Africa.

Appendix A. Supplementary data

Supplementary data to this article can be found online at https://doi.org/10.1016/j.ultsonch.2021.105664.

References

[1] G. Liu, X. Gao, K. Wang, D. He, J. Li, Uniformly mesoporous NiO/NiFe2O4 biphasic nanorods as efficient oxygen evolving catalyst for water splitting, Int. J. Hydrogen Energy. 41 (40) (2016) 17976–17986.
[2] D.H. Youn, Y.B. Park, J.Y. Kim, G. Magesh, Y.J. Jang, J.S. Lee, One-pot synthesis of NiFe layered double hydroxide/reduced graphene oxide composite as an efficient electrocatalyst for electrochemical and photoelectrochemical water oxidation, J. Power Sources. 294 (2015) 437–443.
[3] M. Chatti, A.M. Glushenkov, T. Gengenbach, G.P. Knowles, T.C. Mendes, A.V. Ellis, L. Spiccia, R.K. Hocking, A.N. Simonov, Highly dispersed and disordered nickel–iron layered hydroxides and sulphides: robust and high-activity water oxidation catalysts, Sustain. Energy Fuels. 2 (2018) 1561–1573.
[4] M. Gong, Y. Li, H. Wang, Y. Liang, J.Z. Wu, J. Zhou, J. Wang, T. Regier, F. Wei, H. Dai, An advanced Ni–Fe layered double hydroxide electrocatalyst for water oxidation, J. Am. Chem. Soc. 135 (23) (2013) 8452–8455.
[5] X. Gao, X. Long, H. Yu, X. Pan, Z. Yi, Ni nanoparticles decorated NiFe layered double hydroxide as bifunctional electrochemical catalyst, J. Electrochem. Soc. 164 (6) (2017) H307–H310.
[6] Z. Li, M. Shao, H. An, Z. Wang, S. Xu, M. Wei, D.G. Evans, X. Duan, Fast electrosynthesis of Fe-containing layered double hydroxide arrays toward highly efficient electrocatalytic oxidation reactions, Chem. Sci. 6 (11) (2015) 6624–6631.
[7] Y. Hou, M.R. Lohe, J. Zhang, S. Liu, X. Zhuang, X. Feng, Vertically oriented cobalt selenide/NiFe layered-double-hydroxide nanosheets supported on exfoliated graphene foil: an efficient 3D electrode for overall water splitting, Energy Environ. Sci. 9 (2016) 478–483.
[8] X. Long, J. Li, S. Xiao, K. Yan, Z. Wang, H. Chen, S. Yang, A strongly coupled graphene and FeNi double hydroxide hybrid as an excellent electrocatalyst for the oxygen evolution reaction, Angew. Chemie. 126 (29) (2014) 7714–7718.
[9] W. Liu, J. Bao, M. Guan, Y. Zhao, J. Lian, J. Qiu, L.i. Xu, Y. Huang, J. Qian, H. Li, Nickel–cobalt-layered double hydroxide nanosheet arrays on Ni foam as a bifunctional electrocatalyst for overall water splitting, Dalt. Trans. 46 (26) (2017) 8372–8376.
[10] D.i. Tang, J. Liu, X. Wu, R. Liu, X. Han, Y. Han, H. Huang, Y. Liu, Z. Kang, Carbon quantum dot/NiFe layered double-hydroxide composite as a highly efficient electrocatalyst for water oxidation, ACS Appl. Mater. Interfaces. 6 (10) (2014) 7918–7925.
[11] T. Maiyalagan, K.A. Jarvis, S. Therese, P.J. Ferreira, A. Manthiram, Spinel-type lithium cobalt oxide as a bifunctional electrocatalyst for the oxygen evolution and oxygen reduction reactions, Nat. Commun. 5 (2014) 1–8.
[12] H. Sun, Z. Yan, F. Liu, W. Xu, F. Cheng, J. Chen, Self-supported transition-metal-based electrocatalysts for hydrogen and oxygen evolution, Adv. Mater. 32 (2020) 1806326.
[13] W.T. Hong, M. Risch, K.A. Stoerzinger, A. Grimaud, J. Suntivich, Y. Shao-Horn, Toward the rational design of non-precious transition metal oxides for oxygen electrocatalysis, Energy Environ. Sci. 8 (5) (2015) 1404–1427.
[14] L. Han, S. Dong, E. Wang, Transition-metal (Co, Ni, and Fe)-based electrocatalysts for the water oxidation reaction, Adv. Mater. 28 (42) (2016) 9266–9291.
[15] Y. Shi, Y. Wang, Y. Yu, Z. Niu, B. Zhang, N-doped graphene wrapped hexagonal metallic cobalt hierarchical nanosheet as a highly efficient water oxidation electrocatalyst, J. Mater. Chem. A. 5 (19) (2017) 8897–8902.
[16] H. Zhong, C.A. Campos-Roldán, Y. Zhao, S. Zhang, Y. Feng, N. Alonso-Vante, Recent advances of cobalt-based electrocatalysts for oxygen electrode reactions and hydrogen evolution reaction, Catalysts. 8 (2018) 559.
[17] Z. Lu, H. Wang, D. Kong, K. Yan, P.-C. Hsu, G. Zheng, H. Yao, Z. Liang, X. Sun, Y. Cui, Electrochemical tuning of layered lithium transition metal oxides for improvement of oxygen evolution reaction, Nat. Commun. 5 (2014) 1–7.
[18] G. Mishra, B. Dash, S. Pandey, Layered double hydroxides: A brief review from fundamentals to application as evolving biomaterials, Appl. Clay Sci. 153 (2018) 172–186.
[19] X. Long, Z. Wang, S. Xiao, Y. An, S. Yang, Transition metal based layered double hydroxides tailored for energy conversion and storage, Mater. Today. 19 (4) (2016) 213–226.
[20] L. Wu, L. Yu, X. Xiao, F. Zhang, S. Song, S. Chen, Z. Ren, Recent advances in self-supported layered double hydroxides for oxygen evolution reaction, Research 2020 (2020) 1–17.
[21] M. Gong, Y. Li, H. Wang, Y. Liang, J.Z. Wu, J. Zhou, J. Wang, T. Regier, F. Wei, H. Dai, An advanced Ni-Fe layered double hydroxide electrocatalyst for water oxidation, J. Am. Chem. Soc. 135 (23) (2013) 8452–8455, https://doi.org/10.1021/ja4027715.
[22] Y. Wang, D. Yan, S. El Hankari, Y. Zou, S. Wang, Recent Progress on Layered Double Hydroxides and Their Derivatives for Electrocatalytic Water Splitting, Adv. Sci. 5 (8) (2018) 1800064, https://doi.org/10.1002/advs.v5.810.1002/advs.201800064.
[23] X.-X. Jiang, J.-Y. Xue, Z.-Y. Zhao, C. Li, F.-L. Li, C. Cao, Z. Niu, H.-W. Gu, J.-P. Lang, Ultrathin sulfate-intercalated NiFe-layered double hydroxide nanosheets for efficient electrocatalytic oxygen evolution, RSC Adv. 10 (21) (2020) 12145–12150.
[24] W. Ma, R. Ma, C. Wang, J. Liang, X. Liu, K. Zhou, T. Sasaki, A superlattice of alternately stacked Ni–Fe hydroxide nanosheets and graphene for efficient splitting of water, ACS Nano. 9 (2) (2015) 1977–1984.
[25] H. Chen, X. Huang, L.-J. Zhou, G.-D. Li, M. Fan, X. Zou, Electrospinning synthesis of bimetallic nickel–iron oxide/carbon composite nanofibers for efficient water oxidation electrocatalysis, ChemCatChem. 8 (5) (2016) 992–1000.
[26] L. Lei, D. Huang, C. Zhou, S. Chen, X. Yan, Z. Li, W. Wang, Demystifying the active roles of NiFe-based oxides/(oxy)hydroxides for electrochemical water splitting under alkaline conditions, Coord. Chem. Rev. 408 (2020) 213177, https://doi.org/10.1016/j.ccr.2019.213177.
[27] F. Wang, T. Wang, S. Sun, Y. Xu, R. Yu, H. Li, One-step synthesis of Nickle Iron-layered double hydroxide/reduced graphene oxide/carbon nanofibres composite as electrode materials for asymmetric supercapacitor, Sci. Rep. 8 (2018) 1–10.
[28] L.-F. Zhai, H.-Z. Mao, M. Sun, Fabrication of Ni-Fe LDH/GF anode for enhanced Fe (III) regeneration in fuel cell-assisted chelated-iron dehydrosulfurization process, J. Chem. Technol. Biotechnol. 93 (1) (2018) 80–87.
[29] C. Chen, L. Tao, S. Du, W. Chen, Y. Wang, Y. Zou, S. Wang, Advanced Exfoliation Strategies for Layered Double Hydroxides and Applications in Energy Conversion and Storage, Adv. Funct. Mater. 30 (2020) 1909832.

[30] F. Gu, X. Cheng, S. Wang, X.u. Wang, P.S. Lee, Oxidative Intercalation for Monometallic Ni2+-Ni3+ Layered Double Hydroxide and Enhanced Capacitance in Exfoliated Nanosheets, Small. 11 (17) (2015) 2044–2050.
[31] R. Liu, Y. Wang, D. Liu, Y. Zou, S. Wang, Water-plasma-enabled exfoliation of ultrathin layered double hydroxide nanosheets with multivacancies for water oxidation, Adv. Mater. 29 (2017) 1701546.
[32] M. Yi, Z. Shen, A review on mechanical exfoliation for the scalable production of graphene, J. Mater. Chem. A. 3 (22) (2015) 11700–11715, https://doi.org/10.1039/C5TA00252D.
[33] F. Ali, L. Reinert, J.-M. Levêque, L. Duclaux, F. Muller, S. Saeed, S.S. Shah, Effect of sonication conditions: Solvent, time, temperature and reactor type on the preparation of micron sized vermiculite particles, Ultrason. Sonochem. 21 (3) (2014) 1002–1009, https://doi.org/10.1016/j.ultsonch.2013.10.010.
[34] F. Foroughi, J.J. Lamb, O.S. Burheim, B.G. Pollet, Sonochemical and sonoelectrochemical production of energy materials, Catalysts. 11 (2) (2021) 284, https://doi.org/10.3390/catal11020284.
[35] H. Zheng, M.S. Matseke, T.S. Munonde, The unique Pd@ Pt/C core-shell nanoparticles as methanol-tolerant catalysts using sonochemical synthesis, Ultrason. Sonochem. 57 (2019) 166–171.
[36] B. Pollet, The use of power ultrasound for the production of PEMFC and PEMWE catalysts and low-pt loading and high-performing electrodes, Catalysts. 9 (3) (2019) 246, https://doi.org/10.3390/catal9030246.
[37] B.G. Pollet, The use of ultrasound for the fabrication of fuel cell materials, Int. J. Hydrogen Energy. 35 (21) (2010) 11986–12004, https://doi.org/10.1016/j.ijhydene.2010.08.021.
[38] H.E. Hansen, F. Seland, S. Sunde, O.S. Burheim, B.G. Pollet, Two routes for sonochemical synthesis of platinum nanoparticles with narrow size distribution, Mater. Adv. 2 (6) (2021) 1962–1971, https://doi.org/10.1039/D0MA00909A.
[39] R.S. Yadav, I. Kuřitka, J. Vilcakova, T. Jamatia, M. Machovsky, D. Skoda, P. Urbánek, M. Masař, M. Urbánek, L. Kalina, Impact of sonochemical synthesis condition on the structural and physical properties of MnFe2O4 spinel ferrite nanoparticles, Ultrason. Sonochem. 61 (2020), 104839.
[40] X. Cai, Z. Jiang, X. Zhang, X. Zhang, Effects of tip sonication parameters on liquid phase exfoliation of graphite into graphene nanoplatelets, Nanoscale Res. Lett. 13 (2018) 241.
[41] J. Kim, S. Kwon, D.-H. Cho, B. Kang, H. Kwon, Y. Kim, S.O. Park, G.Y. Jung, E. Shin, W.-G. Kim, Direct exfoliation and dispersion of two-dimensional materials in pure water via temperature control, Nat. Commun. 6 (2015) 1–9.
[42] T.S. Munonde, H. Zheng, M.S. Matseke, P.N. Nomngongo, Y.i. Wang, P. Tsiakaras, A green approach for enhancing the electrocatalytic activity and stability of NiFe2O4/CB nanospheres towards hydrogen production, Renew. Energy. 154 (2020) 704–714.
[43] M.S. Matseke, H. Zheng, Y.i. Wang, Applied Surface Science The ultrasonication boosts the surface properties of CoFe 2 O 4 / C nanoparticles towards ORR in alkaline media, Appl. Surf. Sci. 516 (2020) 146105, https://doi.org/10.1016/j.apsusc.2020.146105.
[44] T.S. Munonde, H. Zheng, P.N. Nomngongo, Ultrasonic exfoliation of NiFe LDH/CB nanosheets for enhanced oxygen evolution catalysis, Ultrason. Sonochem. 59 (2019), 104716.
[45] P. Turner, M. Hodnett, R. Dorey, J.D. Carey, Controlled sonication as a route to in-situ graphene flake size control, Sci. Rep. 9 (2019) 1–8.
[46] J. Huang, P. Xu, D. Cao, X. Zhou, S. Yang, Y. Li, G. Wang, Asymmetric supercapacitors based on β-Ni (OH) 2 nanosheets and activated carbon with high energy density, J. Power Sources. 246 (2014) 371–376.
[47] S. Anantharaj, K. Karthick, M. Venkatesh, T.V.S.V. Simha, A.S. Salunke, L. Ma, H. Liang, S. Kundu, Enhancing electrocatalytic total water splitting at few layer Pt-NiFe layered double hydroxide interfaces, Nano Energy. 39 (2017) 30–43.
[48] J. Fan, Z. Zhao, Z. Ding, J. Liu, Synthesis of different crystallographic FeOOH catalysts for peroxymonosulfate activation towards organic matter degradation, RSC Adv. 8 (13) (2018) 7269–7279.
[49] F. Song, X. Hu, Exfoliation of layered double hydroxides for enhanced oxygen evolution catalysis, Nat. Commun. 5 (1) (2014), https://doi.org/10.1038/ncomms5477.
[50] R. Ma, Z. Liu, K. Takada, N. Iyi, Y. Bando, T. Sasaki, Synthesis and exfoliation of Co2+− Fe3+ layered double hydroxides: An innovative topochemical approach, J. Am. Chem. Soc. 129 (2007) 5257–5263.
[51] Z. Cai, X. Bu, P. Wang, J.C. Ho, J. Yang, X. Wang, Recent advances in layered double hydroxide electrocatalysts for the oxygen evolution reaction, J. Mater. Chem. A. 7 (10) (2019) 5069–5089.
[52] L. Azar, Cavitation in Ultrasonic Cleaning and Cell Disruption, Control. Environ. (2009).
[53] Y.e. Yao, Y. Pan, S. Liu, Power ultrasound and its applications: A state-of-the-art review, Ultrason. Sonochem. 62 (2020) 104722, https://doi.org/10.1016/j.ultsonch.2019.104722.
[54] S.R. Alharbi, M. Alhassan, O. Jalled, S. Wageh, A. Saeed, Structural characterizations and electrical conduction mechanism of CaBi 2 Nb 2 O 9 single-phase nanocrystallites synthesized via sucrose-assisted sol–gel combustion method, J. Mater. Sci. 53 (16) (2018) 11584–11594.
[55] S.B.K. Moorthy, Thin film structures in energy applications, Springer, 2015.
[56] V. Petkov, Pair Distribution Functions Analysis, Charact. Mater. (2012), https://doi.org/10.1002/0471266965.com159.
[57] P.F. Fewster, A new theory for X-ray diffraction, Acta Crystallogr. Sect. A Found. Adv. 70 (3) (2014) 257–282, https://doi.org/10.1107/S205327331400117X.
[58] C. Yang, C. Wöll, IR spectroscopy applied to metal oxide surfaces: adsorbate vibrations and beyond, Adv. Phys. X. 2 (2017) 373–408.
[59] D. Sokol, K. Klemkaite-Ramanauske, A. KHINSKY, K. Baltakys, A. Beganskiene, A. Baltusnikas, J. Pinkas, A. Kareiva, Reconstruction effects on surface properties of Co/Mg/Al layered double hydroxide, Mater. Sci. 23 (2017) 144–149.
[60] R. Elmoubarki, F.Z. Mahjoubi, A. Elhalil, H. Tounsadi, M. Abdennouri, M. Sadiq, S. Qourzal, A. Zouhri, N. Barka, Ni/Fe and Mg/Fe layered double hydroxides and their calcined derivatives: preparation, characterization and application on textile dyes removal, J. Mater. Res. Technol. 6 (2017) 271–283.
[61] L.S. Liji, R. Mehedi, M. Malmivirta, P. Paturi, M. Lastusaari, M.M. Dîrtu, Y. Garcia, P. Fardim, Heteronuclear nanoparticles supported hydrotalcites containing Ni(II) and Fe(III) stable photocatalysts for Orange II degradation, Appl. Clay Sci. 132–133 (2016) 641–649, https://doi.org/10.1016/j.clay.2016.08.016.
[62] X. Xu, F. Song, X. Hu, A nickel iron diselenide-derived efficient oxygen-evolution catalyst, Nat. Commun. 7 (2016) 1–7.
[63] J. Xie, H. Qu, F. Lei, X. Peng, W. Liu, L. Gao, P. Hao, G. Cui, B. Tang, Partially amorphous nickel–iron layered double hydroxide nanosheet arrays for robust bifunctional electrocatalysis, J. Mater. Chem. A. 6 (33) (2018) 16121–16129.
[64] K. Okitsu, Y. Mizukoshi, H. Bandow, Y. Maeda, T. Yamamoto, Y. Nagata, Formation of noble metal particles by ultrasonic irradiation, Ultrason. Sonochem. 3 (3) (1996) S249–S251, https://doi.org/10.1016/S1350-4177(96)00033-8.
[65] M. Kohno, T. Mokudai, T. Ozawa, Y. Niwano, Free radical formation from sonolysis of water in the presence of different gases, J. Clin. Biochem. Nutr. 49 (2) (2011) 96–101, https://doi.org/10.3164/jcbn.10-130.
[66] M.H. Uddin, S.-ichi. Hatanaka, S. Hayashi, Effects of aqueous temperature on sonolysis of bisphenol A: Rate constants increasing with temperature under oxygen, J. Chem. Eng. Japan. 42 (4) (2009) 303–308, https://doi.org/10.1252/jcej.08we233.
[67] R. Ji, R. Pflieger, M. Virot, S.I. Nikitenko, Multibubble Sonochemistry and Sonoluminescence at 100 kHz: The Missing Link between Low- and High-Frequency Ultrasound, J. Phys. Chem. B. 122 (27) (2018) 6989–6994, https://doi.org/10.1021/acs.jpcb.8b0426710.1021/acs.jpcb.8b04267.s001.
[68] A. Šutka, S. Lagzdina, T. Käämbre, R. Pärna, V. Kisand, J. Kleperis, M. Maiorov, A. Kikas, I. Kuusik, D. Jakovlevs, Study of the structural phase transformation of iron oxide nanoparticles from an Fe2+ ion source by precipitation under various synthesis parameters and temperatures, Mater. Chem. Phys. 149-150 (2015) 473–479, https://doi.org/10.1016/j.matchemphys.2014.10.048.
[69] G. Zhang, S. Wang, F. Yang, Efficient adsorption and combined heterogeneous/homogeneous fenton oxidation of Amaranth using supported nano-FeOOH as cathodic catalysts, J. Phys. Chem. C. 116 (5) (2012) 3623–3634, https://doi.org/10.1021/jp210167b.
[70] J.T. Han, J.I. Jang, H. Kim, J.Y. Hwang, H.K. Yoo, J.S. Woo, S. Choi, H.Y. Kim, H. J. Jeong, S.Y. Jeong, Extremely efficient liquid exfoliation and dispersion of layered materials by unusual acoustic cavitation, Sci. Rep. 4 (2014) 5133.
[71] W. Lauterborn, T. Kurz, R. Geisler, D. Schanz, O. Lindau, Acoustic cavitation, bubble dynamics and sonoluminescence, Ultrason. Sonochem. 14 (4) (2007) 484–491.
[72] M.E.G. Lyons, R.L. Doyle, Oxygen evolution at oxidised iron electrodes: A tale of two slopes, Int. J. Electrochem. Sci. (2012).
[73] R.L. Doyle, M.E.G. Lyons, Kinetics and mechanistic aspects of the oxygen evolution reaction at hydrous iron oxide films in base, J. Electrochem. Soc. 160 (2) (2013) H142–H154.
[74] M.S. Burke, M.G. Kast, L. Trotochaud, A.M. Smith, S.W. Boettcher, Cobalt–iron (oxy) hydroxide oxygen evolution electrocatalysts: the role of structure and composition on activity, stability, and mechanism, J. Am. Chem. Soc. 137 (2015) 3638–3648.
[75] R. Li, Y. Guo, H. Chen, K. Wang, R. Tan, B. Long, Y. Tong, P. Tsiakaras, S. Song, Y. Wang, Anion-Cation Double Doped Co3O4 Microtube Architecture to Promote High-Valence Co Species Formation for Enhanced Oxygen Evolution Reaction, ACS Sustain. Chem. Eng. 7 (13) (2019) 11901–11910.
[76] Y. Ma, X. Dai, M. Liu, J. Yong, H. Qiao, A. Jin, Z. Li, X. Huang, H. Wang, X. Zhang, Strongly coupled FeNi alloys/NiFe2O4@ carbonitride layers-assembled microboxes for enhanced oxygen evolution reaction, ACS Appl. Mater. Interfaces. 8 (50) (2016) 34396–34404.
[77] W. Song, Z. Ren, S.-Y. Chen, Y. Meng, S. Biswas, P. Nandi, H.A. Elsen, P.-X. Gao, S. L. Suib, Ni-and Mn-promoted mesoporous Co3O4: a stable bifunctional catalyst with surface-structure-dependent activity for oxygen reduction reaction and oxygen evolution reaction, ACS Appl. Mater. Interfaces. 8 (2016) 20802–20813.
[78] Z. Qiu, C.-W. Tai, G.A. Niklasson, T. Edvinsson, Direct observation of active catalyst surface phases and the effect of dynamic self-optimization in NiFe-layered double hydroxides for alkaline water splitting, Energy Environ. Sci. 12 (2) (2019) 572–581, https://doi.org/10.1039/C8EE03282C.
[79] K. Zhu, H. Liu, M. Li, X. Li, J. Wang, X. Zhu, W. Yang, Atomic-scale topochemical preparation of crystalline Fe3+-doped β-Ni(OH)2 for an ultrahigh-rate oxygen evolution reaction, J. Mater. Chem. A. 5 (17) (2017) 7753–7758, https://doi.org/10.1039/C7TA01408B.
[80] J. Chen, F. Zheng, S.-J. Zhang, A. Fisher, Y. Zhou, Z. Wang, Y. Li, B.-B. Xu, J.-T. Li, S.-G. Sun, Interfacial Interaction between FeOOH and Ni-Fe LDH to Modulate the Local Electronic Structure for Enhanced OER Electrocatalysis, ACS Catal. 8 (12) (2018) 11342–11351, https://doi.org/10.1021/acscatal.8b0348910.1021/acscatal.8b03489.s001.
[81] M.B. Stevens, C.D.M. Trang, L.J. Enman, J. Deng, S.W. Boettcher, Reactive Fe-Sites in Ni/Fe (Oxy)hydroxide Are Responsible for Exceptional Oxygen Electrocatalysis Activity, J. Am. Chem. Soc. 139 (33) (2017) 11361–11364, https://doi.org/10.1021/jacs.7b0711710.1021/jacs.7b07117.s001.
[82] F. Cheng, J. Shen, B. Peng, Y. Pan, Z. Tao, J. Chen, Rapid room-temperature synthesis of nanocrystalline spinels as oxygen reduction and evolution

electrocatalysts, Nat. Chem. 3 (1) (2011) 79–84, https://doi.org/10.1038/nchem.931.
[83] J. Suntivich, K.J. May, H.A. Gasteiger, J.B. Goodenough, Y. Shao-Horn, A perovskite oxide optimized for oxygen evolution catalysis from molecular orbital principles, Science 334 (6061) (2011) 1383–1385, https://doi.org/10.1126/science:1212858.
[84] M. Gong, H. Dai, A mini review of NiFe-based materials as highly active oxygen evolution reaction electrocatalysts, Nano Res. 8 (1) (2015) 23–39, https://doi.org/10.1007/s12274-014-0591-z.
[85] L. Trotochaud, S.L. Young, J.K. Ranney, S.W. Boettcher, Nickel-Iron oxyhydroxide oxygen-evolution electrocatalysts: The role of intentional and incidental iron incorporation, J. Am. Chem. Soc. 136 (18) (2014) 6744–6753, https://doi.org/10.1021/ja502379c.
[86] D. Friebel, M.W. Louie, M. Bajdich, K.E. Sanwald, Y. Cai, A.M. Wise, M.-J. Cheng, D. Sokaras, T.-C. Weng, R. Alonso-Mori, R.C. Davis, J.R. Bargar, J.K. Nørskov, A. Nilsson, A.T. Bell, Identification of highly active Fe sites in (Ni, Fe)OOH for electrocatalytic water splitting, J. Am. Chem. Soc. 137 (3) (2015) 1305–1313, https://doi.org/10.1021/ja511559d.